3-20-2011

Constraining the coalescence rate of supermassive black-hole binaries using pulsar timing

Z. L. Wen

F. A. Jenet

D. Yardley

G. B. Hobbs

R. N. Manchester

CONSTRAINING THE COALESCENCE RATE OF SUPERMASSIVE BLACK-HOLE BINARIES USING PULSAR TIMING

Z. L. Wen[1], F. A. Jenet[2], D. Yardley[3,4], G. B. Hobbs[4], and R. N. Manchester[4]
[1] National Astronomical Observatories, Chinese Academy of Sciences, Jia-20 DaTun Road, ChaoYang District, Beijing 100012, China; zhonglue@bao.ac.cn
[2] Center for Gravitational Wave Astronomy, University of Texas at Brownsville, TX 78520, USA; merlyn@phys.utb.edu
[3] Sydney Institute for Astronomy (SIfA), School of Physics, The University of Sydney, NSW 2006, Australia
[4] CSIRO Astronomy and Space Science, Australia Telescope National Facility, P.O. Box 77, Epping, NSW 1710, Australia

ABSTRACT

Pulsar timing observations are used to place constraints on the rate of coalescence of supermassive black-hole (SMBH) binaries as a function of mass and redshift. In contrast to the indirect constraints obtained from other techniques, pulsar timing observations provide a direct constraint on the black-hole merger rate. This is possible since pulsar timing is sensitive to the gravitational waves (GWs) emitted by these sources in the final stages of their evolution. We find that upper bounds calculated from the recently published Parkes Pulsar Timing Array data are just above theoretical predictions for redshifts below 10. In the future, with improved timing precision and longer data spans, we show that a non-detection of GWs will rule out some of the available parameter space in a particular class of SMBH binary merger models. We also show that if we can time a set of pulsars to 10 ns timing accuracy, for example, using the proposed Square Kilometre Array, it should be possible to detect one or more individual SMBH binary systems.

Key words: early universe – galaxies: statistics – gravitational waves – methods: data analysis – pulsars: general

1. INTRODUCTION

Pulsar timing observations (for a review of the techniques, see Lorimer & Kramer 2005, chapter 8; Edwards et al. 2006) provide a unique opportunity to study low-frequency (10^{-9} to 10^{-7} Hz) gravitational waves (GWs; Sazhin 1978; Detweiler 1979; Bertotti et al. 1983; Hellings & Downs 1983; Foster & Backer 1990; Kaspi et al. 1994; Jenet et al. 2005). Previous work (Romani & Taylor 1983; Kaspi et al. 1994; Lommen 2002; Jenet et al. 2006) placed upper limits on a stochastic background of GWs. These limits were reported in terms of either the amplitude of the GW characteristic strain spectrum, $h_c(f)$, or the normalized GW energy density, $\Omega_{gw}(f)$.

In recent years, researchers have proposed that supermassive black-hole (SMBH) binary systems distributed throughout the universe will be a source of GWs detectable using pulsar timing techniques (e.g., Jaffe & Backer 2003; Wyithe & Loeb 2003; Enoki et al. 2004; Sesana et al. 2004, 2008). The detection, or non-detection, of such GWs provides a constraint on the rate of coalescence of SMBH binary systems. We emphasize that such constraints are model-independent as opposed to the indirect constraints that can be inferred from observed galaxy distributions.

We will show that existing pulsar data sets do not provide stringent constraints on the coalescence rate. However, future data sets from the Parkes Pulsar Timing Array (PPTA; Manchester 2008; Hobbs et al. 2009b) as well as the North American Nano-hertz Observatory for GRAVitational waves (NANOGrav; Jenet et al. 2009) and European Pulsar Timing Array (EPTA; Stappers et al. 2006) projects aim to produce data sets on 20 or more pulsars with rms timing residuals close to 100 ns. In the longer term, we expect that pulsar timing array projects using future telescopes such as the Square Kilometre Array (SKA)[5] will be able to time many hundreds of pulsars with exquisite timing precision.

The outline of this paper is as follows. In Section 2, the physics of GW emission from SMBH binary systems is reviewed together with the effects of GWs on pulsar timing. We describe how to constrain the coalescence rate using two different techniques, one valid when there is a large number of expected sources and the other valid when only a few sources are expected. In Section 3, we show the recent and projected rate constraints for various different observing systems. These observationally constrained rates are then compared to the rates implied by local galaxy-merger observations. The work is summarized in Section 4.

2. CONSTRAINING THE SMBH MERGER RATE

We define an SMBH as a black hole with mass greater than $10^6 \, M_\odot$. There is abundant evidence that such SMBHs exist both nearby (e.g., Kormendy & Richstone 1992; Miyoshi et al. 1995) and at high redshifts $z \sim 6$ (e.g., Fan et al. 2001). Two orbiting SMBHs resulting from a galaxy merger would emit large amplitude GWs. Such GW sources are important targets for space-based detectors such as *LISA* and pulsar timing arrays (e.g., Wyithe & Loeb 2003; Enoki et al. 2004; Sesana et al. 2004). Observational GW astronomy can be used to resolve whether SMBH binary systems form and whether the two black holes can get close enough to emit detectable GWs.

This work focuses on the rate constraints measurable by pulsar timing observations. In order to determine the coalescence rate, one needs to know the expected GW amplitude emitted by an SMBH binary. This is given by (Thorne 1987)

$$h_s = 4\sqrt{\frac{2}{5}} \frac{(GM_c)^{5/3}}{c^4 D(z)} [\pi f(1+z)]^{2/3}, \tag{1}$$

where M_c is the "chirp mass" of the SMBH binary given by $M_c = (M_1 M_2)^{3/5}(M_1 + M_2)^{-1/5}$, M_1 and M_2 are the individual black-hole masses, f is the observed GW frequency, and $D(z)$ is

---
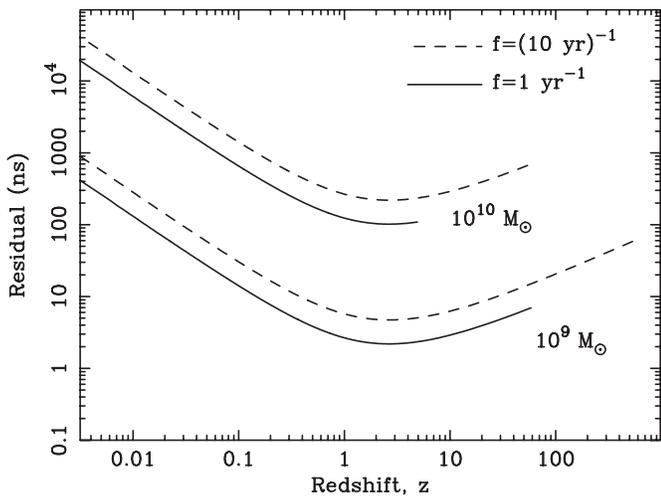
[5] See http://www.skatelescope.org.

Figure 1. Induced timing residual amplitudes vs. redshift of a system with a given observed frequency and chirp mass.

the comoving distance to the system

$$D(z) = \frac{c}{H_0} \int_0^z \frac{dz'}{E(z')}, \tag{2}$$

with $E(z) = \sqrt{\Omega_\Lambda + \Omega_m(1+z)^3}$ for a ΛCDM cosmological model (hereafter we adopt $H_0 = 72$ km s^{-1} Mpc^{-1}, $\Omega_m = 0.3$, and $\Omega_\Lambda = 0.7$). GWs from such a source will induce sinusoidally oscillating arrival-time variations whose amplitude, Δt, is given by (Jenet et al. 2004 and references therein):

$$\Delta t = \frac{h_s}{\omega}[1 + \cos(\theta)] \sin(2\phi) \sin\{\omega D[1 - \cos(\theta)]/2c\}, \tag{3}$$

where ω is the GW frequency in rad s^{-1}, θ is the angle on the sky between the pulsar direction and the GW source direction, ϕ is the GW polarization angle, and D is the distance to the pulsar. The maximum induced timing residual amplitude, h_s/ω, is plotted in Figure 1 as a function of redshift for chirp masses of 10^9 and $10^{10} M_\odot$ and observed GW frequencies of $(1\text{ yr})^{-1}$ and $(10\text{ yr})^{-1}$. The most notable feature in this figure is that these amplitude curves are not monotonically decreasing with increasing redshift. The reason for this is that the observing frequency is held fixed and the frequency in the frame of the emitting system increases with increasing redshift. For a binary system, the emitted GW amplitude increases with increasing frequency. For large z, this increase is faster than the decrease due to increasing comoving distance $D(z)$. Also note that the curves cutoff at large z. This is because there is a maximum orbital frequency allowed before the black holes plunge together. This maximum frequency was taken to be $c^3/(6^{3/2}\pi GM)$ assuming a circular orbit (Hughes 2002). Here, $M = M_1 + M_2$ is the total mass of a binary system.

RMS timing residuals (for a typical 1 hr observation) for the best pulsar data sets are currently around 100 ns. Multiple observations combined with improved systems will bring the effective sensitivity down to around 10 ns. In this case, Figure 1 shows that pulsar timing will be sensitive to individual SMBH binary systems with chirp masses greater than about $10^9 M_\odot$. Figure 1 also shows that this sensitivity extends to large redshifts. This fact greatly increases the chances of detecting individual sources. An ensemble of lower-mass SMBH binary systems will be detectable as a stochastic background if there is a large enough population of sources.

Since pulsar timing techniques are sensitive to SMBH binary systems up to high redshifts, the non-detection of any sources, either individual binaries or a background generated by an ensemble of binary systems, may be used to place a direct constraint on $d^2R/dM_c dz$, the sky-averaged rate of coalescence of binary SMBHs per unit chirp mass, M_c, per unit redshift z. The total number of binary SMBHs with chirp mass between M_c and $M_c + \Delta M_c$ and located between z and $z + \Delta z$ merging between time t and $t + \Delta t$ is given by $\Delta M_c \Delta z \Delta t\, d^2R/dM_c dz$. Constraints placed on this quantity may be used to rule out various binary SMBH formation models.

We present two methods for determining the coalescence rate from pulsar timing data. The first is valid when the rate is high enough that the GWs form a stochastic background (the "stochastic constraint") and there is a large number of sources per resolvable frequency bin. The second method (the "Poissonian constraint") provides an estimate of the coalescence rate when the stochastic constraint does not hold. For a real data set, it is practical first to assume the stochastic constraint, determine the coalescence rate, and check whether the rate is high enough for the assumption to be valid. If not then the Poissonian constraint should be used.

2.1. Stochastic Constraint

Here, it is assumed that a large number of SMBH binary sources form an incoherent background of GWs. The power spectrum of such a background is given by Jaffe & Backer (2003)

$$P(f) = \int_0^\infty \int_0^\infty h_s(f, M_c, z)^2 \frac{d^2R}{dz dM_c} \left(\frac{df}{dt}\right)^{-1} dz dM_c, \tag{4}$$

where $h_s(f, M_c, z)$ is given by Equation (1) and df/dt is the rate of change of the observed GW frequency. For the case of a binary system evolving under general relativity alone, this is given by Peters & Mathews (1963)

$$\frac{df}{dt} = \frac{96}{5} \left(\frac{GM_c}{c^3}\right)^{5/3} (\pi f)^{8/3} f(1+z)^{5/3}. \tag{5}$$

Typically, a stochastic background of GWs is described by its characteristic strain spectrum, $h_c(f)$, which is assumed to take on a power-law form:

$$h_c(f) = A \left(\frac{f}{f_{yr}}\right)^\alpha, \tag{6}$$

where $f_{yr} = 1/(1\text{ yr})$ and A is the characteristic strain at a period of 1 yr. For a background generated by SMBH binaries, $\alpha = -2/3$ in frequency range 10^{-9} to 10^{-7} Hz (Jaffe & Backer 2003; Wyithe & Loeb 2003; Sesana et al. 2004; Enoki et al. 2004). Note that the characteristic strain spectrum is related to the power spectrum by $P(f) = h_c(f)^2/f$.

Pulsar timing data sets provide an upper bound, A_{up}, on A. Such bounds limit the power spectrum of the GW strain. The upper bound, $P_{up}(f)$, may be written as

$$P_{up}(f) = \frac{A_{up}^2}{f_{yr}} \left(\frac{f}{f_{yr}}\right)^{-7/3}. \tag{7}$$

Since this is an upper bound, we have

$$P(f) < P_{up}(f). \tag{8}$$

In order to use Equations (4) and (8) to obtain a constraint on the differential rate of coalescence itself, the integrand is rewritten in an equivalent form

$$P(f) = \int_0^\infty \int_{-\infty}^\infty h_s(f, M_c, z)^2 \frac{d^2 R}{d\lg(1+z)d\lg(M_c)}$$
$$\times \left(\frac{df}{dt}\right)^{-1} d\lg(1+z)d\lg(M_c). \qquad (9)$$

Note that both $d^2 R/d\lg(1+z)d\lg(M_c)$ and df/dt depend on z and M_c, although the explicit dependence is not written. A constraint on $P(f)$ is a direct constraint on the integral in the above expression. In order to obtain an estimate of the upper bound on the integrand, we follow the same line of reasoning used to place constraints on the differential energy density of GWs using bounds from big bang nucleosynthesis (Maggiore 2000). First, we note that the limits in the integral of Equation (9) are from 0 to ∞ for $\lg(1+z)$ and from $-\infty$ to ∞ for $\lg(M_c)$. Consider this integral over a small region bounded by $\lg(M_{c_1})$ to $\lg(M_{c_2})$ and $\lg(1+z_1)$ to $\lg(1+z_2)$. Denote this integral as $P_s(f)$ where

$$P_s(f) = \int_{\lg(M_{c_1})}^{\lg(M_{c_2})} \int_{\lg(1+z_1)}^{\lg(1+z_2)} h_s(f, M_c, z)^2 \frac{d^2 R}{d\lg(1+z)d\lg(M_c)}$$
$$\times \left(\frac{df}{dt}\right)^{-1} d\lg(1+z)d\lg(M_c). \qquad (10)$$

The mean value theorem tells us that there exist values of M_c and z, written as M_c^* and z^*, such that

$$P_s(f) = h_s(f, M_c^*, z^*)^2 \frac{d^2 R}{d\lg(1+z)d\lg(M_c)} \left(\frac{df}{dt}\right)^{-1}$$
$$\times \Delta\lg(1+z)\Delta\lg(M_c), \qquad (11)$$

where $\Delta\lg(1+z) = \lg(1+z_2) - \lg(1+z_1)$ and $\Delta\lg(M_c) = \lg(M_{c_2}) - \lg(M_{c_1})$. Next, we assume that the integrand varies slowly over the region of integration so that $P_s(f)$ does not change much as long as M_c^* and z^* are chosen within this region. From this, we see that $P_s(f)$ is approximately given by

$$P_s(f) \approx h_s(f, M_c, z)^2 \frac{d^2 R}{d\lg(1+z)d\lg(M_c)} \left(\frac{df}{dt}\right)^{-1}$$
$$\times \Delta\lg(1+z)\Delta\lg(M_c) \qquad (12)$$

for any value of $M_c \in [M_{c_1}, M_{c_2}]$ and $z \in [z_1, z_2]$. Next, since the integrand in Equation (9) is positive definite, it follows that

$$P_s(f) \leqslant P(f). \qquad (13)$$

From Equations (7), (8), (12), and (13), we have

$$h_s(f, M_c, z)^2 \frac{d^2 R}{d\lg(1+z)d\lg(M_c)} \left(\frac{df}{dt}\right)^{-1}$$
$$\times \Delta\lg(1+z)\Delta\lg(M_c) \lesssim \frac{A_{up}^2}{f_{yr}} \left(\frac{f}{f_{yr}}\right)^{-7/3}, \qquad (14)$$

where we are free to choose any value for M_c and z provided that the integrand is slowly varying over the appropriate region. Using the known expressions for $h_s(f, M_c, z)$ and df/dt, one can use Equation (14) to obtain a constraint on the differential

rate of coalescence. Assuming $\Delta\lg(M_c) = 1$ and $\Delta\lg(1+z) = 0.2$, the constraint takes the form

$$\frac{d^2 R}{d\lg(1+z)d\lg(M_c)} < 15 A_{up}^2 \frac{c^3 D(z)^2 (1+z)^{1/3}}{(GM_c)^{5/3}} (\pi f_{yr})^{4/3}, \qquad (15)$$

which is independent of frequency. Therefore, a measured bound, A_{up}, can be used directly to constrain the SMBH coalescence rate. Note that, if one believes that the integrand changes more rapidly with z and/or M_c, one can choose a sufficiently small integration range over which this assumption is true and then rescale the above constraint.

This constraint is only valid when there are a large number of sources emitting into the same frequency band at the same time. In order for this to be true, the GW amplitude of each source must be much less than the minimum detectable amplitude as determined by the statistical properties of the pulsar timing data, otherwise a detection would have been made. This reasoning leads to the following constraint: $h_s(f, M_c, z)^2 \ll P_{up}(f)\Delta f$, where Δf is the resolution bandwidth which is taken to be $1/T_{obs}$. For the purposes of making numerical estimates, the following constraint is used:

$$h_s(f, M_c, z)^2 \leqslant 0.1 \frac{P_{up}(f)}{T_{obs}}. \qquad (16)$$

For a fixed chirp mass and frequency, this expression is a constraint on z. The most stringent constraint occurs when $f = 1/T_{obs}$, the lowest observable frequency. Combining the above with Equations (1) and (7) yields the following constraint on the redshift:

$$\frac{(1+z)^{2/3}}{D(z)} \leqslant 0.19 \left(\frac{A_{up}}{10^{-14}}\right) \left(\frac{T_{obs}}{yr}\right)^{4/3} \left(\frac{M_c}{10^8 M_\odot}\right)^{-5/3} Mpc^{-1}. \qquad (17)$$

The factor $(1+z)^{2/3}/D(z)$ decreases with z until $z = 2.65$, where it starts to increase. Hence, there is a bounded redshift interval over which the stochastic constraint is valid. For systems outside of this range, the stochastic rate limit is not valid and the Poisson rate limit discussed in the next section must be employed.

2.2. Poisson Constraint

For this case, the sources are not numerous enough to form a stochastic background, so they must be treated as individual events. Assuming Poissonian statistics for the probability of an event occurring, the probability that no events are detected is given by $e^{-\langle N \rangle}$, where $\langle N \rangle$ is the expected number of events. Since no events are detected in the pulsar timing data, the upper limit on the expected number, $\langle N_* \rangle$, is set so that $e^{-\langle N_* \rangle} = 0.05$. Hence, $\langle N \rangle \leqslant \langle N_* \rangle = 3$. If the actual expected number were greater than 3, then at least one source would have been detected with 95% probability.

Provided that the expected number of events that occur within the resolution bandwidth is less than one, the expected number of detectable events is given by

$$\langle N \rangle = \int \frac{d^2 R}{d\lg(1+z)d\lg(M_c)} \left(\frac{df}{dt}\right)^{-1}$$
$$\times P_d(M_c, z, f) d\lg(1+z)d\lg(M_c)df, \qquad (18)$$

where $P_d(M_c, z, f)$ is the probability of detecting an SMBH binary with chirp mass M_c at a redshift of z with observable
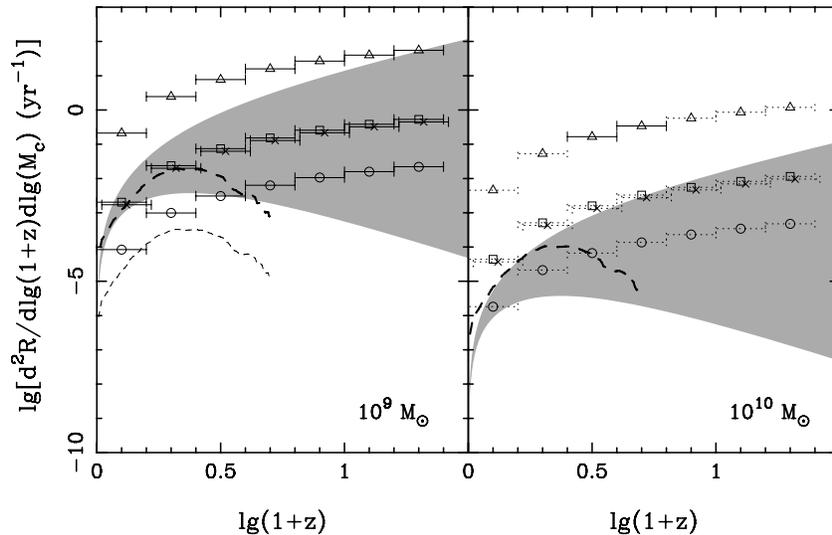
Figure 2. Upper limits on the SMBH binary merger rate determined by the stochastic constraint discussed in Section 2.1 for different data sets: real data published by Jenet et al. (2006, open triangles), simulated data for 20 PSRs–500 ns–10 yr (open squares), 20 PSRs–100 ns–5 yr (crosses), and 20 PSRs–100 ns–10 yr (open circles). The error bar is plotted as a dotted line when the constraint is invalid. The filled gray area represents the expected region for the coalescence rate using the framework of Jaffe & Backer (2003) together with the data from the SDSS (Wen et al. 2009) with an evolution index $-1 < \gamma < 3$. The dashed lines between $0 < \lg(1 + z) < 0.7$ indicate the maximum (thick) and minimum (thin) predicted rates from Sesana et al. (2008, 2009).

frequency f. P_d takes into account non-GW noise sources that can reduce the GW detection efficiency. Following the same argument used in the previous section to obtain an upper bound on the differential rate using an integral constraint, we find that

$$\frac{d^2R}{d\lg(1+z)d\lg(M_c)} < \frac{15}{\int \left(\frac{df}{dt}\right)^{-1} P_d(M_c, z, f)df}. \quad (19)$$

As with the stochastic constraint, it is assumed that $\Delta \lg(M_c) = 1$ and $\Delta \lg(1 + z) = 0.2$. This constraint should be appropriately rescaled if the integrand in Equation (18) varies over shorter intervals.

The above constraint requires a knowledge of P_d, the probability of detecting an SMBH binary system using pulsar timing data. The P_d is calculated using a method similar to that in Yardley et al. (2010). For our analysis, we use a Monte Carlo simulation together with the data analysis pipeline (Hobbs et al. 2009a) used to search for GWs in real and simulated pulsar timing data. We use a Neyman–Pearson decision technique together with a Lomb periodogram to determine the probability of detection. For a set of N_p pulsars, the power spectra of the timing residuals are calculated and added together. This summed power spectrum is used as the detector. We determine noise levels and hence detection thresholds for each frequency channel so that the false alarm rate for a detection is 0.001 across the entire power spectrum. The detection thresholds are found by producing 100,000 fake data sets by shuffling the input timing residuals, carrying out standard pulsar timing fits and forming the summed power spectrum.

Once the thresholds are determined, the probability of detecting a GW with a given strain amplitude is calculated as follows. A GW strain amplitude A and frequency f are chosen (this procedure is repeated on a logarithmically spaced grid where A ranges from 10^{-16} to 10^{-10} and f ranges from $1/(30 \text{ yr})$ to $1/(2 \text{ weeks})$). The GW polarization properties are chosen to be consistent with GWs emitted from a binary system and simulated as described in Hobbs et al. (2009a). The direction of the GW wave vector is chosen from a distribution that is uniform on the sky while its polarization is drawn from a distribution of

randomly oriented binary systems. The induced timing residuals from this GW source are added to a shuffled version of the original residuals and the summed periodogram is calculated. This is repeated 1000 times and $P_d(A, f)$ is given by the number of times that the GW was detected (i.e., produced power above the threshold) divided by the total number of trials.

3. RESULTS AND DISCUSSION

The expressions in the previous sections can be used to provide constraints on the rate of coalescence with any measurement of A_{up} (for the stochastic case) or P_d (for the Poissonian case). Here we discuss the implications of the value of A_{up} presented by Jenet et al. (2006), use the same data set to determine P_d, and simulate data sets predicting possible future timing residuals. For these future data sets, we simulate (1) a realistic goal for existing pulsar timing array experiments (20 pulsars, timed with an rms timing residual of 500 ns over 10 yr), (2) the goal of the PPTA project (20 pulsars, timed with an rms of 100 ns over five years), and (3) a more challenging goal of 20 pulsars, timed with an rms of 100 ns over 10 yr. The rms timing residuals that will be achieved with future telescopes, such as the SKA, are not easy to determine. It may be possible to time a few pulsars with exquisite precision (with rms timing residuals of 10 ns) but other unmodeled noise processes may make this difficult or impossible. We therefore also simulate the following possible future data sets: (4) 100 pulsars timed at 100 ns over 5 yr, (5) the same for 10 yr, (6) 20 pulsars timed at 10 ns for 10 yr, and (7) the same for 100 pulsars.

Figures 2 and 3 plot the stochastic constraints given by Equation (15) for the different observing scenarios. The horizontal error bars indicate the region of $\lg(1 + z)$ over which the constraint is placed. The solid error bars indicate that the stochastic constraint is valid, while the dotted error bars indicate that the stochastic validity condition is violated over the whole range. Table 1 gives the valid redshift range for each data set and chirp mass. As discussed above, it was assumed that $\Delta \lg(1+z) = 0.2$ and $\Delta \lg(M_c) = 1$ in order to calculate the constraints shown. The constraints should be rescaled if other values are assumed.
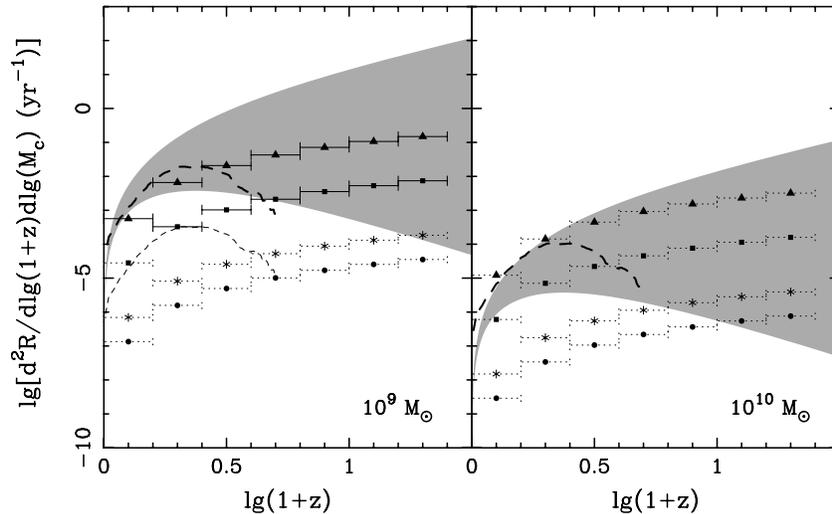
Figure 3. Same as Figure 2, but for simulated data sets: 100 PSRs–100 ns–5 yr (filled triangles), 100 PSRs–100 ns–10 yr (filled squares), 20 PSRs–10 ns–10 yr (stars), and 100 PSRs–10 ns–10 yr (filled circles).

Table 1
Upper Limits on the Amplitude of the Stochastic GW Background

Data Set	A_{up}	Valid Redshift Range	
		$(10^9 \, M_\odot)$	$(10^{10} \, M_\odot)$
PPTA data (Jenet et al. 2006)	1.1×10^{-14}	0.01–180.08	1.78–4.02
20 PSRs–500 ns–10 yr	1.1×10^{-15}	0.03–602.60	–
20 PSRs–100 ns–5 yr	9.9×10^{-16}	0.07–294.97	–
20 PSRs–100 ns–10 yr	2.2×10^{-16}	0.14–115.98	–
20 PSRs–10 ns–10 yr	2.0×10^{-17}	–	–
100 PSRs–100 ns–5 yr	5.7×10^{-16}	0.14–121.46	–
100 PSRs–100 ns–10 yr	1.3×10^{-16}	0.27–45.30	–
100 PSRs–10 ns–10 yr	8.8×10^{-18}	–	–

Note. Symbol "–" indicates that there is no valid range for that scenario.

For redshifts where the stochastic technique is not valid, the Poissonian constraint may be used. Using $P_d(A, f)$, Equation (1) is used to calculate $P_d(M_c, z, f)$ and then the right-hand side of Equation (19) is evaluated numerically to determine the constraint on the differential coalescence rate. The results are plotted versus redshift for different chirp masses in Figures 4 and 5. We note that the recently published PPTA data set, that with 20 pulsars timed with an rms of 500 ns over 10 yr, and that with 20 pulsars timed with an rms of 100 ns over 5 yr are not constraining for SMBH binaries with $M_c = 10^9 \, M_\odot$ and are therefore not plotted in the left-hand panel of Figure 4.

In order to understand how constraining the pulsar rate limits are, plots of the expected SMBH binary coalescence rate are also shown in the figures. Several authors have developed analytical and numerical techniques to estimate the coalescence rate of SMBH binaries. Here, we compare the measured rate constraints to the rates predicted by the models of Jaffe & Backer (2003) and Sesana et al. (2008, 2009). For the case of Jaffe & Backer (2003), the differential rate of SMBH binary coalescence is given by

$$\frac{d^2 R}{d \lg(1+z) d \lg(M_c)} = \frac{4\pi c}{H_0} \frac{D(z)^2}{\lg(e) E(z)} \frac{\Phi(\lg(M_c))}{n} \Re(z), \quad (20)$$

where $\Re(z)$ is the total merger rate of SMBH binaries per unit comoving volume, $\Phi(\lg(M_c))$ is the chirp mass distribution of merging SMBH binaries, and n is the number density of SMBH

binaries given by $n = \int \Phi(\lg(M_c)) d \lg(M_c)$. It is assumed that the merger rate of SMBH binaries is given by a fraction, ϵ, of the galaxy-merger rate and that the rate evolves as a power of $(1+z)$. Hence, one can write $\Re(z) = \epsilon \Re_g(0)(1+z)^\gamma$, where $\Re_g(0)$ is the local merger rate of galaxy pairs and γ is the evolution index which is thought to be within the range $-1 < \gamma < 3$ (e.g., Patton et al. 2002; Lin et al. 2004; Kartaltepe et al. 2007; Lin et al. 2008). Wen et al. (2009) determined $\Re_g(0)$ and $\Phi(\lg(M_c))$ for luminous galaxies by analyzing data from the Sloan Digital Sky Survey (SDSS; York et al. 2000). They found that $\Re_g(0) = (1.0 \pm 0.4) \times 10^{-5} \, \mathrm{Mpc}^{-3} \, \mathrm{Gyr}^{-1}$ and

$$\lg[\Phi(\lg(M_c))] = (21.7 \pm 4.2) - (3.0 \pm 0.5) \lg(M_c / M_\odot).$$
$$(21)$$

Note that Wen et al. (2009) showed that the rate implied by Equation (20) together with the above estimates for $\Re_g(0)$ and $\Phi(\lg(M_c))$ yields an expected characteristic strain spectrum consistent with other published estimates of h_c (Wyithe & Loeb 2003; Sesana et al. 2004; Enoki et al. 2004; Sesana et al. 2008).

For the Sesana et al. (2008, 2009) models, the rate may be estimated from the following expression:

$$\frac{d^2 R}{d \lg(1+z) d \lg(M_c)} = \frac{d \dot{N}_m}{d \lg(M_c)} \frac{1}{\dot{N}} \frac{d \dot{N}}{dz} \frac{(1+z)}{\lg(e)}, \quad (22)$$

where $d \dot{N}_m / d \lg(M_c)$ is the mass function of coalescing SMBHs in the notation of Sesana et al. (2009), and $d \dot{N}/dz$ is the SMBH binary coalescence rate per unit redshift in the notation of Sesana et al. (2008). The constant $\dot{N}$ is given by

$$\dot{N} = \int_0^4 \frac{d \dot{N}}{dz} dz. \quad (23)$$

The limits of the integral are set by the data presented in Figure 12 of Sesana et al. (2008). The factor of $(1 + z)/\lg(e)$ is used to convert the differential dz into $d \lg(1+z)$. From Figure 1 of Sesana et al. (2009), we can estimate the maximum and minimum predicted values of the mass function $d \dot{N}_m / d \lg(M_c)$ over the four models presented therein. We find that, for $M_c = 10^9 \, M_\odot$, the mass function lies between $10^{-4} \, \mathrm{yr}^{-1}$ and $6 \times 10^{-3} \, \mathrm{yr}^{-1}$. These correspond to the "Tr-SA" and the "La-SA"
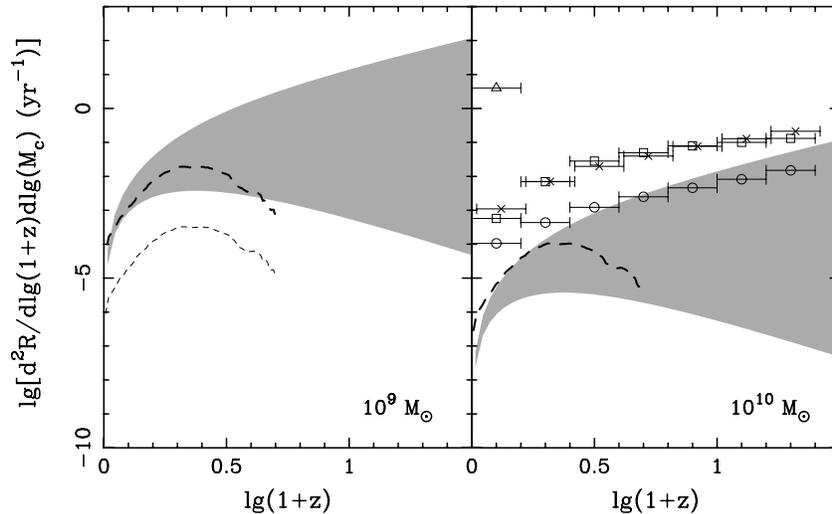
Figure 4. Upper limits on the SMBH merger rate using the Poissonian constraint discussed in Section 2.2 for different data sets: real data from Jenet et al. (2006) (open triangle), 20 PSRs–500 ns–10 yr (open squares), 20 PSRs–100 ns–5 yr (crosses), and 20 PSRs–100 ns–10 yr (open circles). The filled gray area represents the expected region for the coalescence rate using the framework of Jaffe & Backer (2003) together with the data from the SDSS (Wen et al. 2009) with an evolution index, $-1 < \gamma < 3$. The dashed lines between $0 < \lg(1+z) < 0.7$ indicate the maximum (thick) and minimum (thin) predicted rates from Sesana et al. (2008, 2009). Note that no upper limits on the coalescence rate are obtainable for SMBH of $M_c = 10^9 M_\odot$ at these sensitivities.
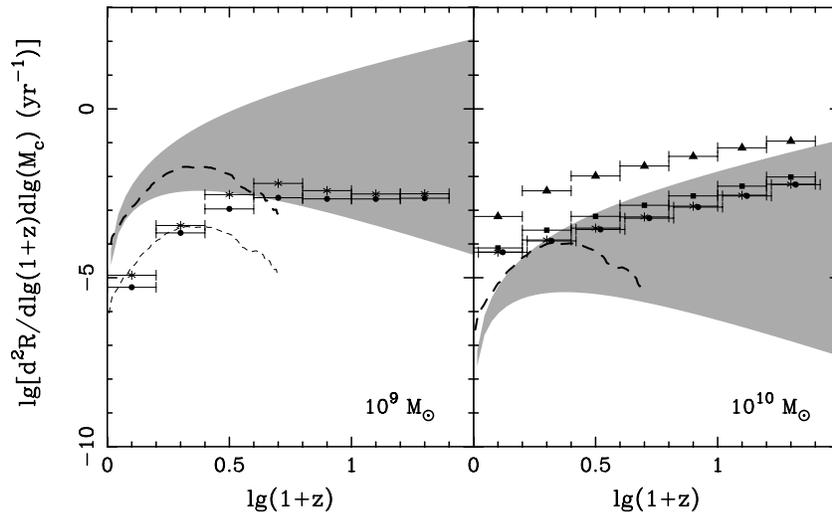

Figure 5. Same as Figure 4, but for the following simulated data sets: 100 PSRs–100 ns–5 yr (filled triangles), 100 PSRs–100 ns–10 yr (filled squares), 20 PSRs–10 ns–10 yr (stars), and 100 PSRs–10 ns–10 yr (filled circles).

models, respectively, as discussed in Sesana et al. (2009). For the case of $M_c = 10^{10} M_\odot$, the predicted range lies between 0 and 3×10^{-5} yr^{-1}. These values also correspond to the "Tr-SA" and "La-SA" models, respectively. For the SMBH binary coalescence rate per unit redshift, $d\dot{N}/dz$, we used the data presented in Figure 12 of Sesana et al. (2008). The three possible models shown are all approximately within a factor of two of each other. For definiteness, we chose the prediction based on the BVRhf model. In this case, $\dot{N} \approx 0.05$ yr^{-1}.

Figures 2 and 3 plot the pulsar timing stochastic constraint together with the expected rates for the theoretical models considered above as a function of redshift for different chirp masses. The Poissonian constraint is plotted together with the expected rates in Figures 4 and 5. Since there are few to no close SMBH binary systems detected near $z = 0$, it can be assumed that $\epsilon \approx 1$. The only free parameter remaining in the Jaffe & Backer (2003) model is the evolution index which determines the SMBH binary merger rate as a function of redshift. The gray regions in Figures 2–5 give the range of expected merger

rates for $-1 < \gamma < 3$. The maximum and minimum rates found using the Sesana et al. (2008, 2009) models are shown as thick dashed and thin dashed lines, respectively. Note, since the minimum predicted rate for $M_c = 10^{10} M_\odot$ is not presented by the Sesana et al. models, this curve is not shown. Overall, the upper bounds obtained by pulsar timing data do not constrain the parameters of the SMBH binary merger models discussed in this paper beyond their currently accepted ranges. For the PPTA goal (20 pulsars timed at 100 ns rms accuracy for 5 yr), the results imply that either a detection will be made or $\gamma < 1.7$ at redshift $z < 3$. In order to place constraints that will limit the models of Sesana et al. (2008, 2009) as well as the Jaffe & Backer (2003) model with $\gamma < -1$, one must either time 100 pulsars with 100 ns rms timing precision or 20 pulsars at the 10 ns level, both of which should be possible with the proposed SKA project.

The Poissonian constraint is only useful for constraining the properties of the most massive SMBH binaries since these systems are rarer than their less massive counterparts and emit

a stronger GW signal. Figure 4 shows that the ideal PPTA extended to 10 yr of observations will just be able to place useful limits for the most massive systems if γ were in the larger end of its possible range. It will be more interesting when we can time pulsars to the 10 ns level. Here, the Poissonian constraint will be well below that expected for $\sim 10^9 \, M_\odot$ SMBH binaries from both the Sesana et al. (2008, 2009) and Wen et al. (2009) models. Hence, with 20 pulsars timed with 10 ns rms timing accuracy for 10 yr, we have a very good chance of detecting an individual source or will place very stringent constraints on models of SMBH binary formation and evolution. These conclusions are consistent with the recent work of Sesana et al. (2009).

4. SUMMARY

We have shown that pulsar timing observations may be used to place constraints on the rate of coalescence of binary SMBHs distributed throughout the universe. Two types of constraints were considered: a stochastic constraint and a Poissonian constraint. The stochastic constraint, which is based on a detection algorithm for the stochastic GW background, gives lower rates but it is only valid when the expected amplitude for an individual source is much less than the minimum detectable amplitude. When this is not the case, the Poissonian constraint must be used. This constraint is based on a continuous-wave detection algorithm and it assumes that the number of coalescence events is distributed according to a Poisson distribution. In both cases, it is assumed that the differential rate of coalescence varies sufficiently slowly over a range of chirp masses and redshifts. The precise numerical value of the constraint depends on the size of the interval over which the rate is assumed to be nearly constant.

The implied rate constraint obtained from recently published data together with rate constraints expected from future possible observing scenarios was compared to theoretical rates calculated from different models. It was shown that 20 pulsars timed with an accuracy of 100 ns, the goal of the PPTA project, will place stringent constraints on the semi-empirical models based on the work of Jaffe & Backer (2003) and Wen et al. (2009). The upper end of the range of backgrounds produced by SMBH population synthesis models (Sesana et al. 2008, 2009) would be detectable by the PPTA goal sensitivity, but higher sensitivity will be needed to further constrain these models if the GW background is not detected. It was also shown that if future observations can time a pulsar with 10 ns accuracy, a direct detection of one or more individual sources is highly likely.

REFERENCES

Bertotti, B., Carr, B. J., & Rees, M. J. 1983, MNRAS, 203, 945
Detweiler, S. 1979, ApJ, 234, 1100
Edwards, R. T., Hobbs, G. B., & Manchester, R. N. 2006, MNRAS, 372, 1549
Enoki, M., Inoue, K. T., Nagashima, M., & Sugiyama, N. 2004, ApJ, 615, 19
Fan, X., et al. 2001, AJ, 122, 2833
Foster, R. S., & Backer, D. C. 1990, ApJ, 361, 300
Hellings, R. W., & Downs, G. S. 1983, ApJ, 265, L39
Hobbs, G., et al. 2009a, MNRAS, 394, 1945
Hobbs, G. B., et al. 2009b, PASA, 26,103
Hughes, S. A. 2002, MNRAS, 331, 805
Jaffe, A. H., & Backer, D. C. 2003, ApJ, 583, 616
Jenet, F. A., Hobbs, G. B., Lee, K. J., & Manchester, R. N. 2005, ApJ, 625, L123
Jenet, F. A., Lommen, A., Larson, S. L., & Wen, L. 2004, ApJ, 606, 799
Jenet, F. A., et al. 2006, ApJ, 653, 1571
Jenet, F., et al. 2009, arXiv:0909.1058
Kartaltepe, J. S., et al. 2007, ApJS, 172, 320
Kaspi, V. M., Taylor, J. H., & Ryba, M. F. 1994, ApJ, 428, 713
Kormendy, J., & Richstone, D. 1992, ApJ, 393, 559
Lin, L., et al. 2004, ApJ, 617, L9
Lin, L., et al. 2008, ApJ, 681, 232
Lommen, A. N. 2002, in Neutron Stars, Pulsars, and Supernova Remnants, ed. W. Becker, H. Lesch, & J. Trümper (Garching bei München: Max-Plank-Institut für extraterrestrische Physik), 114
Lorimer, D. R., & Kramer, M. 2005, Handbook of Pulsar Astronomy (Cambridge: Cambridge Univ. Press)
Maggiore, M. 2000, Phys. Rep., 331, 283
Manchester, R. N. 2008, in AIP Con. Proc. 983, 40 Years of Pulsars: Millisecond Pulsars, Magnetars and More, ed. C. Bassa et al. (Melville, NY: AIP), 584
Miyoshi, M., et al. 1995, Nature, 373, 127
Patton, D. R., et al. 2002, ApJ, 565, 208
Peters, P. C., & Mathews, J. 1963, Phys. Rev., 131, 435
Romani, R. W., & Taylor, J. H. 1983, ApJ, 265, L35
Sazhin, M. V. 1978, SvA, 22, 36
Sesana, A., Haardt, F., Madau, P., & Volonteri, M. 2004, ApJ, 611, 623
Sesana, A., Vecchio, A., & Colacino, C. N. 2008, MNRAS, 390, 192
Sesana, A., Vecchio, A., & Volonteri, M. 2009, MNRAS, 394, 2255
Stappers, B. W., Kramer, M., Lyne, A. G., D'Amico, N., & Jessner, A. 2006, Chin. J. Astron. Astrophys. Suppl., 6, 020000
Thorne, K. S. 1987, in Gravitational Radiation, Three Hundred Years of Gravitation, ed. S. W. Hawking & W. Israel (Cambridge: Cambridge Univ. Press), 330
Wen, Z. L., Liu, F. S., & Han, J. L. 2009, ApJ, 692, 511
Wyithe, J. S. B., & Loeb, A. 2003, ApJ, 590, 691
Yardley, D. R. B., et al. 2010, MNRAS, 407, 669
York, D. G., et al. 2000, AJ, 120, 1579